Ground-Based Scanning Radiometer Measurements During the Water Vapor Intensive Operational Period 2004: A Valuable New Dataset for the Study of the Arctic Atmosphere

D. Cimini, M. Klein, and E.R. Westwater, and V. Leuski
CIRES, University of Colorado
Boulder, Colorado

A.J. Gasiewski, M. Klein, E.R. Westwater, and S. Dowlatshahi
NOAA – Enivonrmental Technology Laboratory
Boulder, Colorado

S. Dowlatshahi
Science and Technology Corporation
Hampton, Virginia

Introduction

The importance of accurate measurements of column amounts of water vapor and cloud liquid has been well documented (Clough et al. 1999). Although several technologies have been investigated to measure these column amounts, microwave radiometers (MWRs) have been used operationally by the Department of Energy's Atmospheric Radiation Measurement (ARM) Program for passive retrievals of precipitable water vapor (PWV) and integrated cloud liquid (ICL). Extremely dry conditions, with PWV less than 3 mm, commonly occur in polar regions during the winter months and accurate measurements of the PWV during such dry conditions are needed to improve our understanding of the regional radiation energy budgets. Under these conditions, the relative accuracy of MWRs, or perhaps of radiosondes, may not be sufficient for quantitative modeling of radiative transfer. To compare several technologies for measuring PWV, an experiment was conducted by the National Aeronautics and Space Administration (NASA) Goddard Space Flight Center (GSFC) and the National Oceanic and Atmospheric Administration (NOAA), Environmental Technology Laboratory (ETL) at the ARM Climate Research Facility (ACRF) North Slope of Alaska (NSA) locale during March of 1999 (Westwater et al. 2001; Racette et al. 2005). Results from this experiment showed the promise of millimeter wavelength radiometers for measuring low amounts of water vapor, but several important questions related to radiometric accuracy and its verification remained unanswered. Consequently, another experiment was conducted in 2004 at the ACRF NSA site near Barrow, Alaska, to address some of these important questions. This paper is one of three papers to be published in the Proceedings of the 2005 ARM Science Team meeting describing the experiment, a new instrument, and showing preliminary results. This work describes the instrument while the other two papers focused on comparisons of radiosonde data (Mattioli et al. 2005) and on millimeter wavelength forward-model studies (Westwater et al. 2005).

The Microwave System Development Division of the NOAA ETL has developed a new instrument, the ground-based scanning radiometer (GSR). The GSR is based on an original design that takes advantage of the experience collected from previous arctic experiments (Westwater et al. 2001) and from the development of NOAA ETL aircraft instrumentation (Gasiewski et al. 1997). The GSR design provides a list of features that are very appealing for arctic research:

- observations at multiple frequencies (26 channels) that extend from microwave to infrared range
- observations at multiple angles (continuous elevation scans from 15° to 165°)
- three stages of calibration (internal references, external targets, and tip curve) for accurate measurements during clear and cloudy conditions
- deployment of submillimeter-wave channels that are very sensitive to low content of liquid and water vapor
- information on cloud depolarization (4 polarimetric channels)
- capability of monitoring simultaneously the main thermodynamic properties of the atmosphere (temperature, humidity, and liquid water content)

The GSR was deployed for the first time during the Arctic Winter Radiometric Experiment Water Vapor Intensive Operative Period (IOP) (Westwater et al. 2004; 2005), held from March 10 to April 9, 2004, at the ACRF site in Barrow, Alaska (71° N, 156° W). About a month of data was collected during the coldest and driest period of the Arctic winter. The primary purpose of the GSR deployment was to measure temperature, water vapor, and cloud properties, at cold (-20° to -55°C) and dry (integrated water vapor < 5 mm) conditions. The major goal was to demonstrate that millimeter-wave radiometers can substantially improve water vapor observations during the Arctic winter.

System Design and Experimental Set-up

The GSR system is depicted, without its protective cover, in Figure 1. The core of the GSR consists of a cylindrical drum, called scanhead, which is able to spin 360°over its axis. The scanhead is mounted on a sliding trolley that can be moved in and out of the main housing. Located inside the housing are the boxes for power and radiometer control (bottom) and two external targets for calibration purposes (top). The scanhead contains six independent radiometers, receiving radiation through separate lens antennas located on the same plate, as pictured in Figure 2. The diameters of the lens antennas were chosen to have beamwidth ranging approximately from 1.8° to 3.5°. Thus, while the scanhead is rotating, all the antennas are pointing in the same direction simultaneously. Each radiometer contains a filter bank to split the radiation in different channels, resulting in 11 single-passband channels in the 50-56 GHz region, 2 double-passband dual-polarized channels (H and V) at 89 GHz, 7 double-sideband channels around the 183.3 GHz water vapor absorption line, 2 double-passband dual-polarized channels at 340 GHz, and 3 double-sideband channels around the strong water vapor line at 382 GHz, as listed in Table 1. Other information, as channel bandwidth, sideband offset, and radiometric sensitivity, as

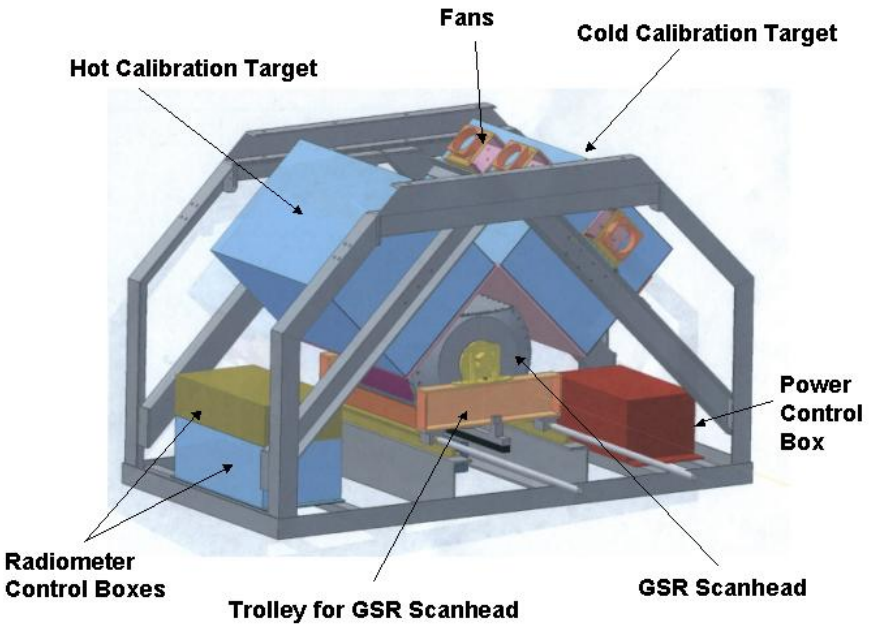

Figure 1. Design of the ground-based scanning radiometer (GSR) without its protective cover.

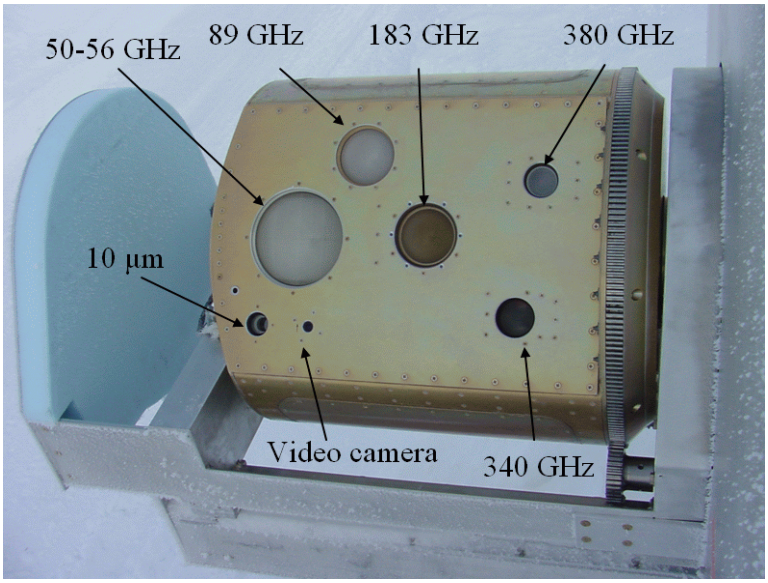

Figure 2. The GSR scanhead during the 2004 Water Vapor IOP, with the lens antennas indicated for each radiometer.

measured in the laboratory, are included in Table 1. Note that the bandwidth for double-sideband channels indicates the 3dB halfwidth for each of the two sidebands, which are shifted from the nominal central frequency of ± the sideband offset Δf. The remaining radiometer consists in an infrared broadband channel at 10.6 micrometers.

Table 1. Central frequency (f_o, GHz), bandwidth (B, GHz), and sensitivity (, K) for GSR microwave channels.

	50-56 GHz			89 GHz			183 GHz			340 GHz			380 GHz		
#chn	**f_o**	**B**	**σ**	**f_o**	**B**	**σ**	**f_o**	**B**	**σ**	**f_o**	**B**	**σ**	**f_o**	**B**	**σ**
01	50.3	0.18	0.09	89 V	1.9	0.04	183.3±0.55	0.3	0.21	340 V	4.75	0.14	380.2±4.0	0.9	0.13
02	51.76	0.40	0.06	89 H	1.9	0.04	183.3±1.0	0.5	0.17	340 H	4.75	0.14	380.2±9.0	2.0	0.11
03	52.62	0.30	0.08				183.3±3.0	0.9	0.13				380.2±17.0	2.0	0.18
04	53.29	0.36	0.07				183.3±4.7	1.4	0.10						
05	53.84	0.19	0.09				183.3±7.0	2.0	0.08						
06	54.4	0.22	0.09				183.3±12.0	3.0	0.07						
07	54.95	0.30	0.08				183.3±16.0	4.0	0.06						
08	55.52	0.18	0.09												
09	56.02	0.25	0.08												
10	56.21	0.50	0.18												
11	56.32	0.50	0.17												

The complete set of GSR microwave channels was selected for the simultaneous retrieval of atmospheric temperature profile, water vapor content, cloud liquid path, and cloud depolarization ratio. In particular, the 50-56 GHz channels are located in the strong oxygen absorption complex and allow for atmospheric temperature estimates (Westwater 1993). The submillimeter-wave channels (183 to 380 GHz) are very sensitive to low water vapor content and allow for accurate observations in the extremely dry and cold conditions typical of the Arctic. The horizontal (H) and vertical (V) polarization channels at 89 and 340 GHz are located in fairly transparent atmospheric regions (windows) and thus allow the study of arctic clouds properties through the measurement of the absorption and depolarization ratio (Dowlatshahi et al. 2005).

The two external targets in Figure 1 are identical and were especially designed for the GSR. Each box contains pyramidal shaped absorbing foam, designed to provide maximum absorption in the direction of the GSR scanhead. Also, the dimensions of each pyramid were chosen so as to maximize absorption over the entire band of GSR frequencies. The microwave emission temperature of the targets is thus precisely calculable using measurements of the physical temperature of the foam. The boxes are thermally stable, but are kept at different temperatures, providing the two reference points needed for complete calibration. The temperature of each target is continuously measured by 16 thermistors, distributed along the volume to monitor temperature gradients and fluctuations.

The GSR was installed at the ARM "Great White" site on March 9, 2004, and collected continuous observations up to April 9, 2004, yielding about a month of data. A picture of the GSR during the first deployment is shown in Figure 3. The whole system is enclosed in the protective cover, leaving clearance for the scanhead to slide out of the housing on the trolley. The GSR was mounted on the north-east corner of the skydeck, which is the platform supporting the operational ARM NSA instruments. With this experimental set-up, the GSR scanhead performed continuous scans along the westeast direction. The GSR has a flexible and software programmable angular-scanning sequence, which was repeated every 2 minutes during the experiment. The sequence starts with the scanhead being inside the calibration house and viewing the hot calibration target for 4 seconds. Then, the scanhead rotates towards the cold target, remaining inside the calibration house, again for 4 seconds. In the next step, the trolley slides out of the calibration house and moves to the atmospheric-scanning

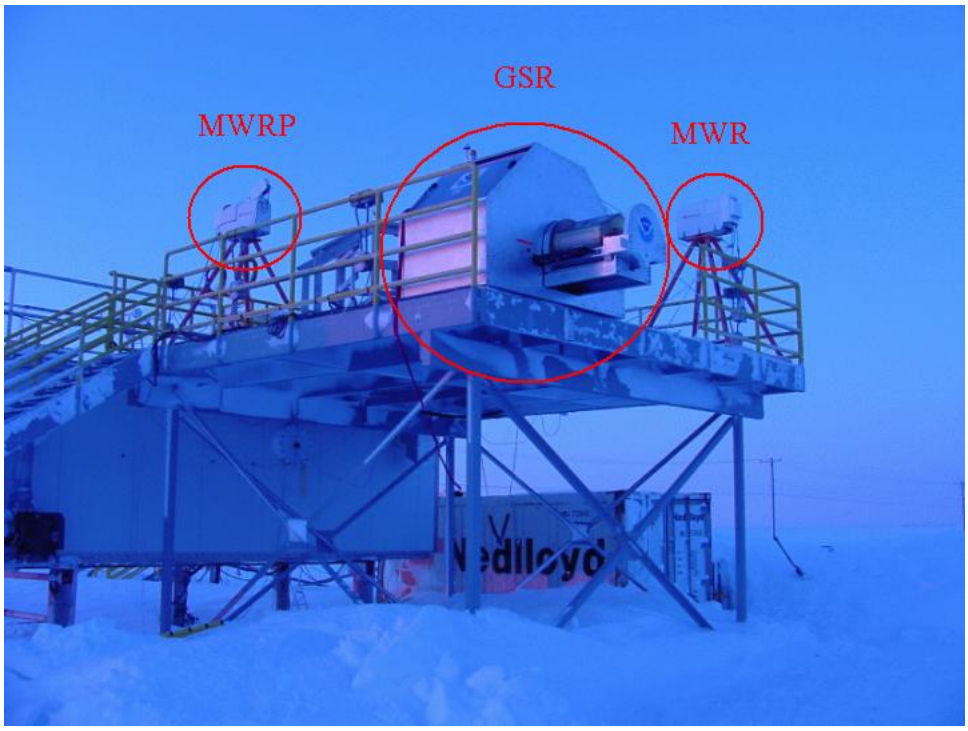

Figure 3. The experimental set-up on the skydeck during the 2004 Water Vapor IOP. The GSR was located by the operational ARM MWRs, the MWR, and the MWE profiler (MWRP).

position. In this position, the scanhead rotates from about 15° to 165° elevation angle, stopping at selected angles (dwells) corresponding to 3, 2.5, 2.0, 1.5, 1.0 air mass. Between the air mass dwells, the scanhead moves to the next scan position while continuously collecting data. Thus, during one complete cycle the radiometers acquire both continuous and dwell observations of the atmosphere plus two-point calibration data. The GSR basic integration and record time was set to about 15 ms.

Mode of Operation and Calibration

The calibration is a key issue for MWRs. A variety of methods are used to calibrate microwave radiometers, which usually rely on internal references (Dicke 1946; Hach 1968), external targets (Ulaby et al. 1981), or atmospheric homogeneity (Han and Westwater 2000). Unfortunately, none of these methods alone is able to establish accurately the complete end-to-end calibration of a MWR. For this reason, MWRs are usually calibrated using a combination of two or more methods (Corbella et al. 2002). In particular, the GSR was designed to allow three stages of calibration, following the three methods introduced above, to provide a high level of absolute accuracy.

I. Internal Calibration

Each GSR radiometer is equipped with an independent switch, located between the antenna and the receiver. During normal operation, the input of each receiver is alternatively switched between the external scene and two internal references. In the case of 55- and 89-GHz radiometers, we use a tri-port

ferrite circulator as a switch, a termination (noise attenuator) as cold reference, and a noise diode as hot reference. On the other hand, for frequencies above 150 GHz, no suitable electric switches exist. Thus, for 183, 340, and 380 GHz radiometers, an electromechanical calibration system using a rotating mirror placed near the antenna and two targets maintained at different temperatures was developed at NOAA ETL. For each of the GSR channels, the calibration coefficients, gain and offset, are estimated via the standard hot-cold method (Ulaby et al. 1981). Because the radiometers spend about half of the time looking at internal loads, the duty cycle is reduced to ½.

II. External Calibration

The internal calibration discussed in the previous section does not include any contribution by the components that are located before the input switch, such as the lens, the antennas, and waveguides. The contribution of these components can be measured in laboratory, but might vary during the deployment because of different reasons, including, but not limited to, temperature fluctuations and small particles over the lens. Therefore, such a contribution needs to be monitored and taken into account during the overall calibration; this can be done by pointing the radiometers towards external references that would include all the components in the calibration process. The GSR system includes two external reference targets (Figure 1). During normal operation, the GSR scanhead points alternatively towards the sky and the two targets, providing a complete end-to-end calibration every cycle, set to 2 minutes during the experiment. The brightness temperature (Tb) of the scene view is obtained from the measured voltages via the standard hot-cold method.

III. Tipping Curve Calibration

The tipping curve method relies on a linear relationship between atmospheric opacity (τ) and air mass (a) for frequency with low absorption (τ <0.5 Np) under the assumption of horizontally-stratified atmosphere. By relating τ, estimated by measurements of Tb, and theoretical values of a at two or more elevation angles, the tipping curve method can provide an adjustment of a single calibration parameter, as carefully discussed by (Han and Westwater 2000). During the sky observations, the GSR antennas scan the atmosphere from 15° to 165° elevation angle, thus allowing the application of the tipping curve method to the channels with relatively low opacity. In the case of GSR, we apply tipping curve method to 50.3, 89 (both H and V), 183±12, 183±15, and 340 (both H and V) GHz channels, including the correction for finite beamwidth described in (Han and Westwater 2000). During clear-sky periods, tipping curve correction is available every scan, i.e. once every 2 minutes.

This last step might seem somewhat redundant, since the complete end-to-end calibration is provided by internal and external calibrations. Conversely, it is highly desirable and extremely useful for checking, and eventually correcting for, other effects that might have been initially neglected, such as angular misalignment or uncertainty in the external target emissivity. In fact, we use the tipping curve method to fine tune the external target emissivity (ε), which is initially set to 0.995.

The quality of the tip curve is checked, discarding cases in which the correlation coefficient of the linear fit is lower than 0.99 (Liljegren 2000). From the set of tipping curve realizations that passed the quality check we compute the parameter ε. The value of ε computed using the tipping curve method is then used also to the remaining channels, assuming that the value of ε changes only slightly with frequency.

The value of ε computed at 50.3 GHz is used for all of the 55-GHz radiometer's channels, while values computed at 340 GHz are used also for the 380 GHz, because none of the 380-GHz channels has absorption weak enough to allow tipping curve.

The implementation of these three steps of calibration in cascade is expected to provide a high level of accuracy during both clear and cloudy conditions.

IV. Settings

During the first deployment of the GSR, the following settings were adopted. The temperature of the external cold target was left floating with ambient temperature (from –40° to –20°C), while the external hot target temperature was kept close to 70°C, covering about 100°C of dynamical range for calibration. A typical time series of GSR observations is shown in Figure 4 for the 51.76-GHz channel; the raw voltage has been calibrated following the steps discussed in Sections I-III, while the measurements during internal reference observations have been removed. The top panel shows Tb measured during a period covering about two complete scans, while in the bottom panel we find the hardware trigger (HT) signal, which associates a different integer for each scanhead position. Referring to Figure 4, a complete cycle is the following:

1. A new scan begins with the scanhead inside the housing, observing the external hot target for 4 seconds (H). The corresponding HT value is 1, as shown in the bottom panel.

2. The scanhead moves towards the next position. The HT value is 3, which means the scanhead is rotating while inside the housing.

3. The scanhead observes the external cold target for 4 seconds (C), which is indicated by the HT value, 2.

4. The scanhead moves to the next position (HT=3), while the trolley moves out of the housing.

5. The trolley reaches the sky-scan position. The scanhead starts to scan in the west direction (indicated by HT=6), stopping at selected dwell positions (HT=11) for 2 seconds. The dwell positions indicated by a, b, c, d, and e correspond to 3.5, 3.0, 2.5, 2.0, and 1.5 air mass, respectively. Moreover, the scanhead collects continuous observations when moving from one dwell to the next.

6. The scanhead reaches the zenith position, indicated by f, and dwells for 2 seconds. Zenith position corresponds to 1 air mass, where the observed Tb shows a minimum.

7. The scanhead starts the east scan (HT=9), stopping at five selected dwell positions (HT=11), corresponding to 1.5, 2.0, 2.5, 3.0, and 3.5 air mass (g, h, i, j, k). The observed Tb increases with the increasing air mass.

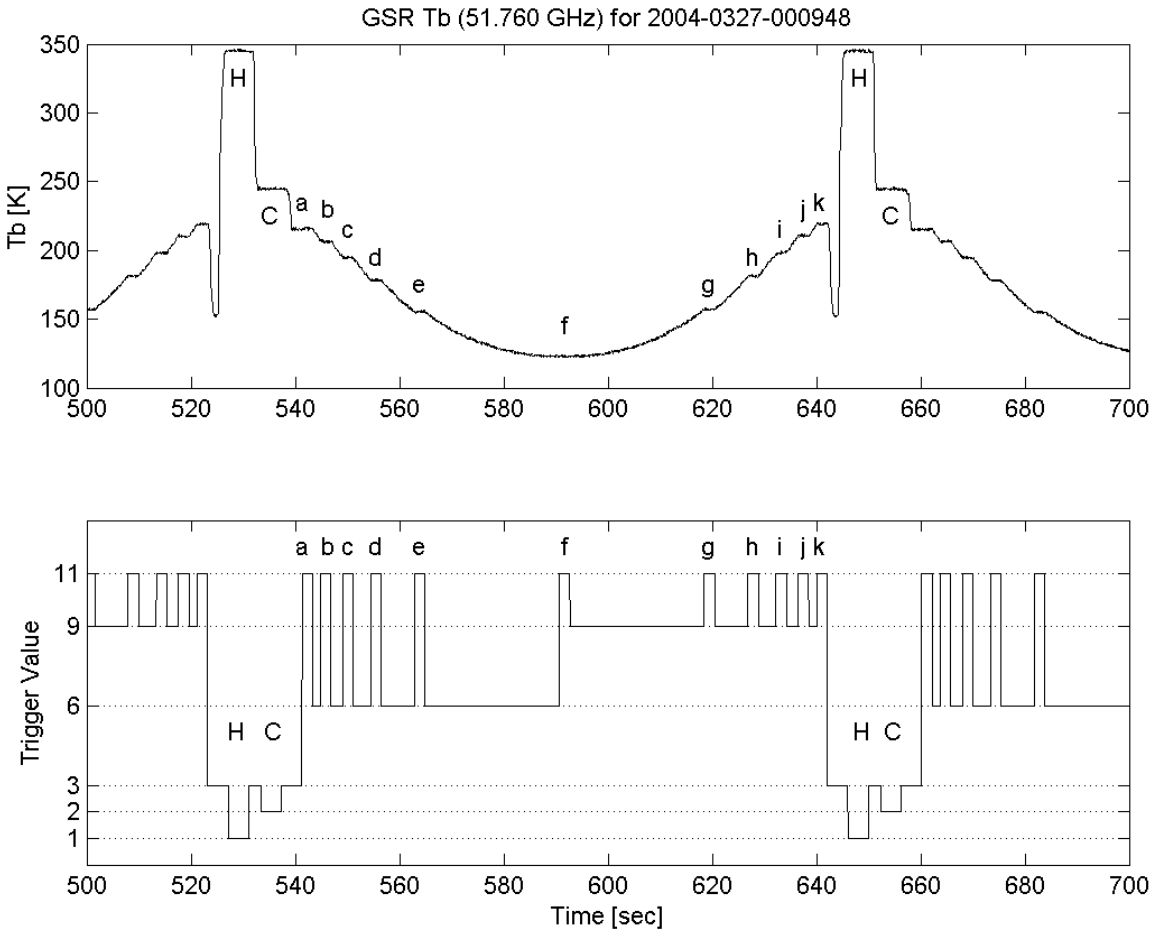

Figure 4. Times series of GSR observations at 50.3 GHz (top), and hardware trigger value indicating scanning position (bottom).

8. The scanhead moves towards the next angular position, while the trolley moves back into the housing (HT=3). The observed Tb shows a sharp decrease due to the scanhead rotation outside the housing, and then a rapid increase when the scanhead is finally back to initial position (HT=1), which corresponds to hot target observation (H).

During the Arctic Winter Radiometric Experiment, the period required to complete the entire cycle was set to 2 minutes.

Preliminary Results

During the Arctic Winter Radiometric Experiment, the GSR worked for a month side-by-side with the NSA operational instruments, such as the dual-channel MWR, and the twelve-channel MWRP, as pictured in Figure 3. Selected preliminary results are shown in this section.

During normal operation, the GSR continuously performs atmospheric scans, acquiring measurements at 26 channels. Note that across the spectral range of GSR channels the atmospheric opacity differs by about 2 orders of magnitude. For this reason, we expect to see Tb as low as 15 K for transparent channels (e.g., 89 GHz), while as high as saturation (~250 K) for very opaque channels (e.g. 56.6, 183±0.5, 380±4 GHz). In Figure 5, for example, three consecutive atmospheric scans, as observed by the GSR 55 GHz channels, demonstrate both angular and spectral signatures. Channels corresponding to low absorption (e.g. 50.3 GHz) show a large dynamical range during the atmospheric scan, with a Tb minimum at zenith. For channels with moderate absorption (e.g. 53.8 GHz), there is a substantial decrease in the dynamical range, although the minimum Tb is still at zenith. For very opaque channels (e.g. 56.325 GHz), the absorption is so strong that radiation comes mainly from lower levels, where a temperature inversion is present; thus, Tb shows a maximum at zenith.

A first comparison of GSR with radiosonde observations (RAOBs) is shown Figure 6, in terms of measured and simulated zenith downwelling Tb. The GSR measurements are shown in colors, while the simulated Tbs, computed from RAOBs at GSR frequencies using the absorption model described by Rosenkranz (1998), are indicated with black stars interpolated with a solid line just to highlight the diurnal trend. Although this is a rather qualitative comparison, we can generally say there is a satisfactory agreement between measurements and simulations. Also shown in Figure 6 are the Tb measured by the ARM MWR at 23.8- and 31.6-GHz channels. In theory, the atmospheric opacity changes of about two orders of magnitude when moving from the 22 GHz water vapor line to the next two higher frequency lines, i.e. 183 and 380 GHz. Therefore, in the dry arctic conditions, we do expect small variations in PWV to cause a much larger response at 183 and 380 GHz with respect to 20-30 GHz. Indeed, the total variation of Tb does not exceed 1.5 K for both the MWR channels, while can be as high as 30 K for millimeter- and submillimeter-wave channels. By simply dividing the variation in Tb by the variation in PWV (as retrieved by an independent unit, the MWRP), we can give a rough estimate of the sensitivity of these channels to small changes in PWV. Using these data, we find 12.8, 385, 442, 514 K/cm for 23, 183±7, 340, and 380±17 GHz, respectively. However, millimeter- and submillimeter-wave channels show non-linear response for higher values of PWV. Thus, these sensitivity estimates are intended only for the range of linearity, which in turn depends on the channel's opacity.

An interesting feature of the GSR data is definitely the continuous-in-angle scan of the atmosphere. This feature gives the possibility to compare measurements with observations at different elevation angles, opening a new prospective for the study of absorption models.

In particular, we want to focus on just two of the GSR channels (53.845 and 54.95 GHz), because they overlap almost completely with two channels (53.85 and 54.94 GHz) operating on the MWRP. Thus, in Figure 7 we compare Tb simulated from a RAOB with GSR and MWRP measurements at these two pairs of channels in the range of elevation angles scanned during the experiment. It is evident that measurements and simulations agree fairly well, likely within the total uncertainty. Although the information content of a continuous scan needs to be analyzed further, it is evident that the GSR catches angular features that are missed by the MWRP, whose scan is limited to few dwell positions per side. In the scanned angular range, the GSR continuous-in-angle scanning provides as much information as the one simulated from the RAOB profiles. In other words, each of the GSR channels provides the maximum information content obtainable by a ground-based single-channel radiometer.

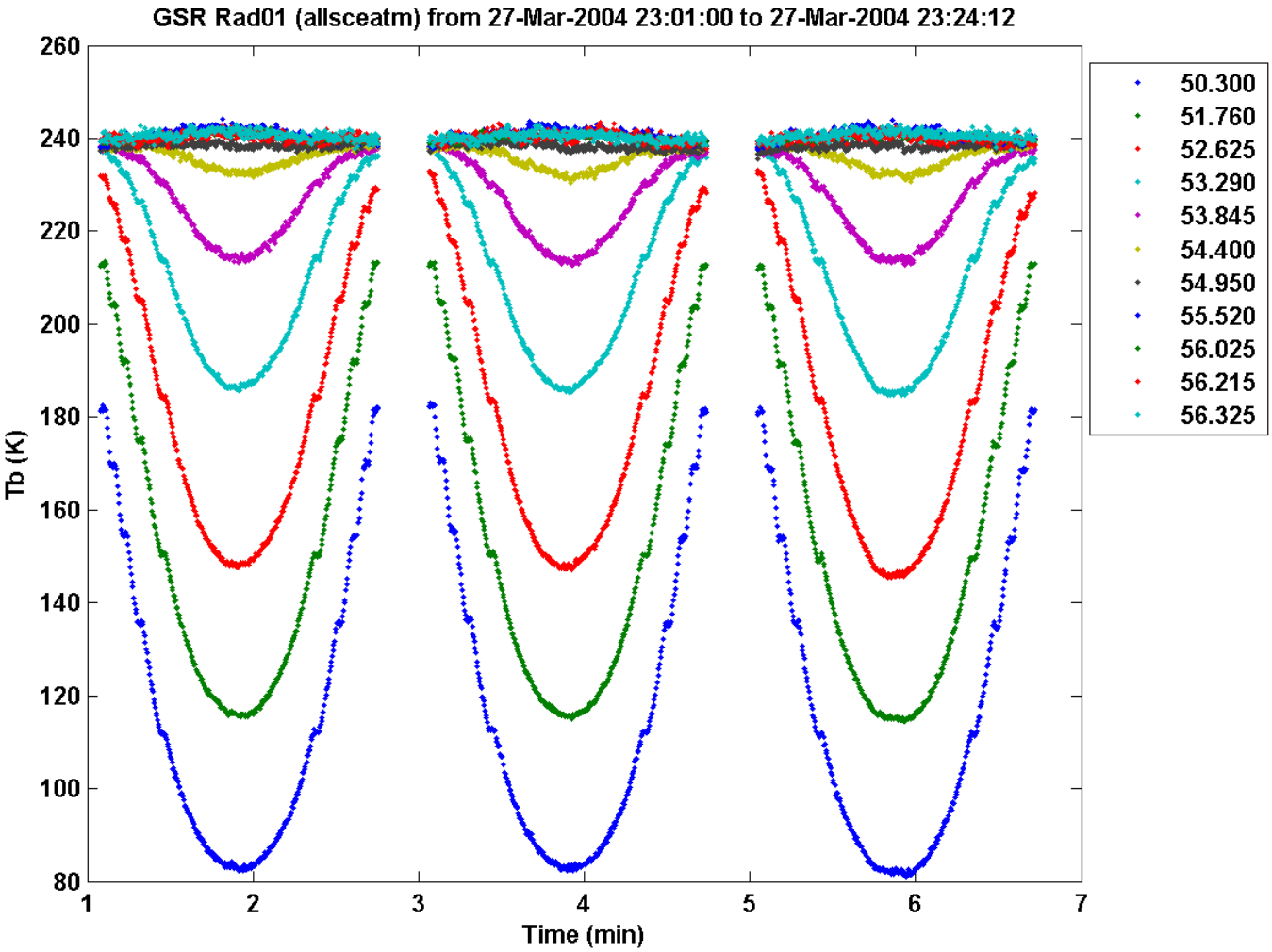

Figure 5. Three consecutive atmospheric scans as observed by GSR 55-GHz channels. The angular and spectral signature of these measurements provide an unprecedent information content. Each scan takes about 2 minutes.

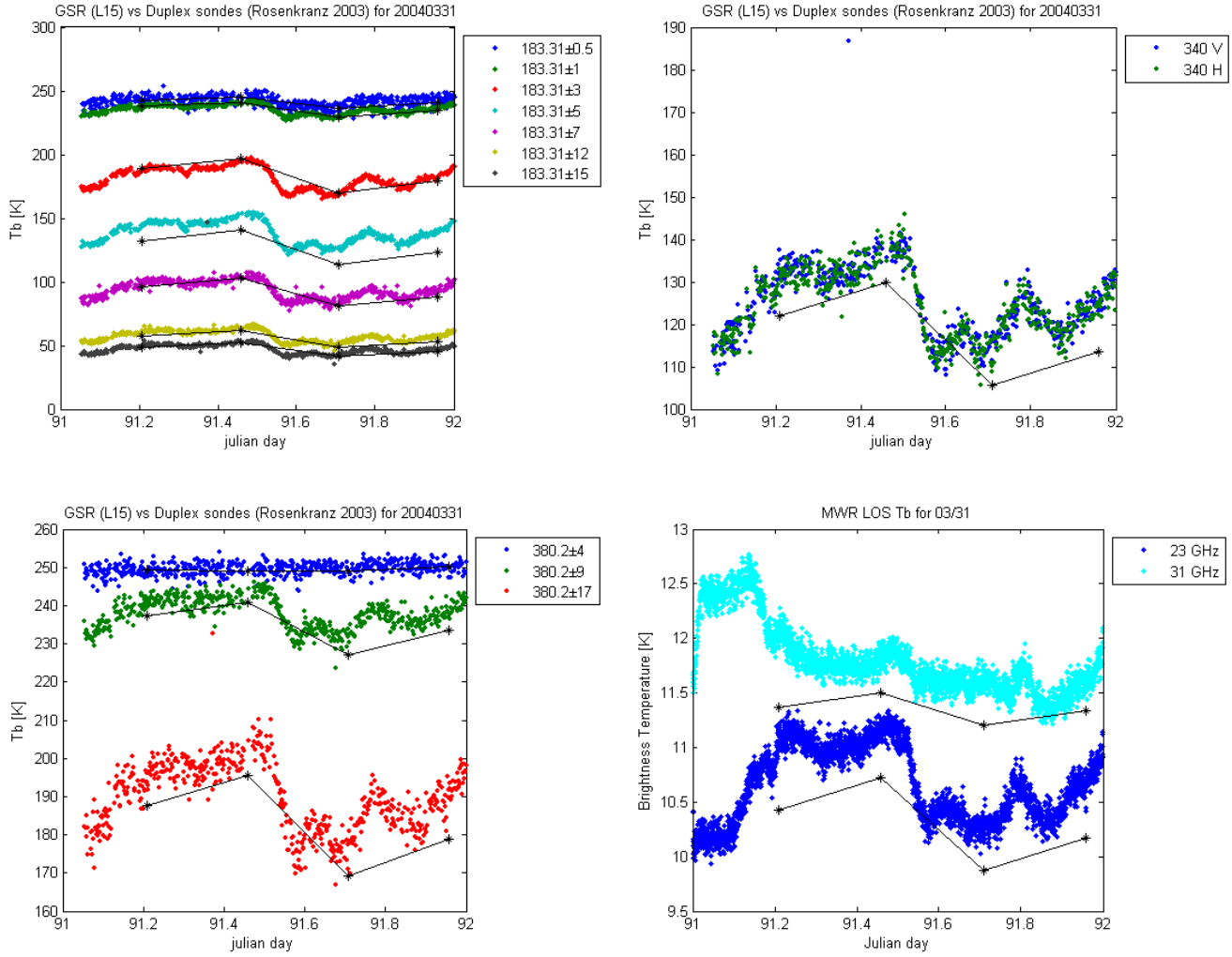

Figure 6. 24-hour time series of GSR and MWR Tbs. Note the 1 K drop at 23.8 GHz around 91.5 UTC; the corresponding gradient shown by submillimeter-wave channels is of the order of 30 K. Simulations based on Rosenkranz 1998 model are indicated with black stars.

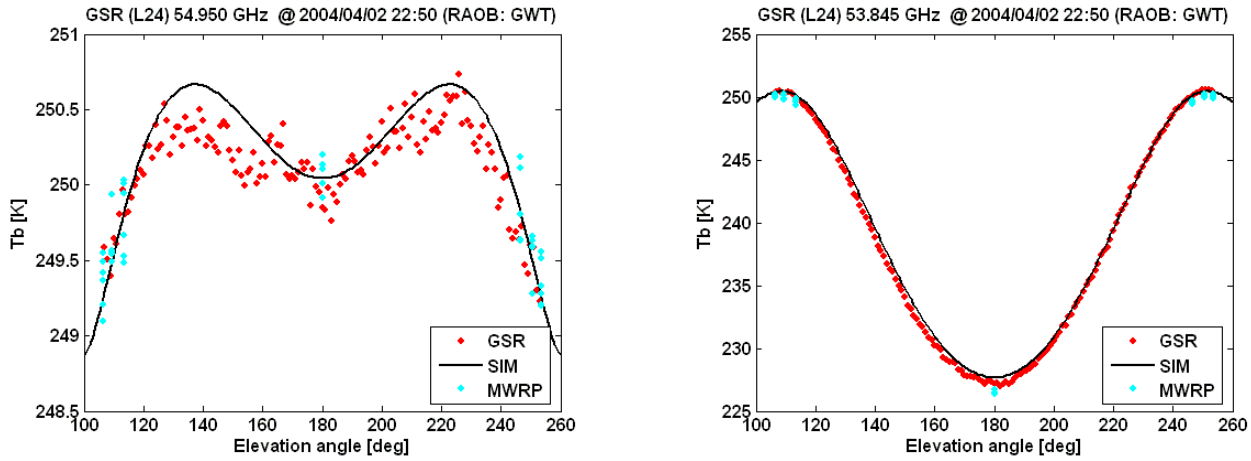

Figure 7. Comparison between simulated and measured Tb during elevation scan. The black line indicates the simulations based on radiosonde observations, while red and cyan dots represent simultaneous GSR and MWRP measurements, respectively.

Summary, Conclusions, and Future Plans

A new instrument, the GSR, was developed by NOAA ETL and deployed for the first time during the 2004 Water Vapor IOP. The GSR ran continuously for 30 days, collecting atmospheric scans under a large variety of conditions. The GSR data presented in this paper are preliminary. Some adjustments to the calibration procedure are still ongoing, to meet the best possible accuracy achievable with this instrument. However, the preliminary results are very encouraging because confirm the expectations about the GSR performances. As expected, all of the GSR channels are suitable for atmospheric observations in the cold, dry arctic environment. The fact that in those atmospheric conditions, sensitive channels do not saturate and show a large signal-to-noise ratio makes them very appealing for the accurate retrieval of very low water vapor content in the Arctic. Moreover, the dual-polarization of window channels gives an opportunity to study the depolarization ratio caused by water, ice, or mixed-phase clouds. The time series of zenith Tb presented in Figure 6 are also very promising.

All the water vapor channels are highly correlated and show a large sensitivity to change in water vapor content. The GSR channels were shown to be more than 20 times more sensitive to small changes in PWV than the conventional instruments used by ARM.

The GSR data provide an unprecedent spectral and angular information content, which opens up new prospective in the ground-based passive remote sensing of the arctic atmosphere. The use of GSR data for the retrieval of atmospheric properties is currently in progress. Our future research will focus on the study of atmospheric absorption model, the development of retrieval techniques with millimeter- and submillimeter-waves, and finally the comparison and coupling of GSR data with measurements from other remote sensing instruments.

Acknowledgements

The work presented in this paper was sponsored by the Environmental Sciences Division of the Department of Energy as a part of their Atmospheric Radiation Measurement Program.

Corresponding Author

Domenico Cimini, Domenico.Cimini@noaa.gov

References

Clough, SA, PD Brown, DD Turner, TR Shippert, JC Liljegren, DC Tobin, HE Revercomb, and RO Knuteson. 1999. "Effect of the Calculated Spectral Surface Radiances due to MWR Scaling of Sonde Water Vapor Profiles." In *Proceedings of Ninth Atmospheric Radiation Measurement (ARM) Program Science Team Meeting*, March 14-18. U.S. Department of Energy.

Corbella, I, AJ Gasiewski, M Klein, V Leuski, AJ Francavilla, and JR Piepmeier. 2002. "On-board accurate calibration of dual-channel radiometers using internal and external references." *IEEE Transactions of the Geosciences Remote Sensing* 50, 7.

Dicke, RH. 1946. "The measurement of thermal radiation at microwave frequencies." *Review of Scientific Instruments* Vol. 17, pp.268-279, July.

Dowlatshahi, SG, AJ Gasiewski, T Uttal, M Klein, ER Westwater and D Cimini. 2005. "Detection of Arctic Cloud Ice Properties Using Submillimeter-wave Radiometers." In *Proceedings of the Eighth Conference on Polar Meteorology and Oceanography, 85th AMS Annual Meeting*, January 9-13.

Gasiewski, AJ, JR Piepmeier, RE McIntosh, CT Swift, JR Carswell, WJ Donnelly, E Knapp, ER Westwater, VI Irisov, LS Fedor, and DC Vandemark. 1997. "Combined High-Resolution Active and Passive Imaging of Ocean Surface Winds from Aircraft." In *International Geoscience and Remote Sensing Symposium*, Singapore, August 3-8.

Hach, JP. 1968. "A Very Sensitive Airborne Microwave Radiometer Using Two Reference Temperatures." *IEEE Transactions Microwave Theory and Techniques* Vol. 16, No.9.

Han, Y, and ER Westwater. 2000. "Analysis and improvement of tipping calibration for ground-based microwave radiometers." *IEEE Transactions Geoscience Remote Sensing* 38, 1260-1277.

Liljegren, JC. 2000. "Automatic self-calibration of ARM microwave radiometers, in Microwave Radiometry and Remote Sensing of the Earth's Surface and Atmosphere." Utrecht: P. Pampaloni and S. Paloscia, Eds., VSP Press, pp. 433–443.

Mattioli, V, ER Westwater, D Cimini, JS Liljegren, BM Lesht, S Gutman, and F Schmidlin. 2005. "Analysis of Radiosonde and PWV data from the 2004 North Slope of Alaska Arctic Winter Radiometric Experiment." In *Proceedings of the Fifteenth Atmospheric Radiation Measurement (ARM) Program Science Team Meeting*, March 14-18. U.S. Department of Energy.

Racette P, ER Westwater, Y Han, A Gasiewski, M Klein, D Cimini, W Manning, E Kim, J Wang, and P Kiedron. 2005. "Measuring Low Amounts of Precipitable Water Vapor Using Millimeter-wave Radiometry." *Journal of Atmospheric and Oceanic Technology*, in press.

Rosenkranz, PW. 1998. "Water vapor microwave continuum absorption: a comparison of measurements and models." *Radio Science* 33:919-928.

Ulaby, FT, RK Moore, and AK Fung. 1981. Microwave remote sensing: Active and passive, Vol. 1. Addison-Wesley Publishing Company, Reading, Massachusetts.

Westwater, ER. 1993. "Ground-based Microwave Remote Sensing of Meteorological Variables," in *Atmospheric Remote Sensing by Microwave Radiometry*, J. Wiley & Sons, Inc., M. Janssen (ed.), 145-213.

Westwater, ER, PE Racette, D Cimini. 2001. "The Artic Winter Millimeter-Wave Radiometric Experiment: Summary, Conclusion and Recommendations." In *Proceedings of Eleventh Atmospheric Radiation Measurement (ARM) Science Team Meeting*, March 19-23.

Westwater ER, M Klein, V Leuski, AJ Gasiewski, T Uttal, DA Hazen, D Cimini, V Mattioli, BL Weber, S Dowlatshahi, JA Shaw, JS Liljegren, BM Lesht, and BD Zak. 2004. Initial Results from the 2004 North Slope of Alaska Arctic Winter Radiometric Experiment." In *Proceedings IEEE Transactions Geoscience Remote Sensing*, Anchorage, Alaska.

Westwater, ER, D Cimini, V Mattioli, M Klein, V Leuski, AJ Gasiewski, S Dowlatshahi, JS Liljegren, BM Lesht, and JA Shaw. 2005. "Microwave and Millimeter Wave Forward Modeling Results from the 2004 North Slope of Alaska Arctic Winter Radiometric Experiment." In *Proceeding of the Fifteenth Atmospheric Radiation Measurement (ARM) Science Team Meeting*, March 14-18. U.S. Department of Energy.